Magnetic structure of $Ba(TiO)Cu_4(PO_4)_4$ probed using spherical neutron polarimetry

P. Babkevich,[1,*] L. Testa,[1] K. Kimura,[2] T. Kimura,[3] G. S. Tucker,[1,4] B. Roessli,[4] and H. M. Rønnow[1]

[1]*Laboratory for Quantum Magnetism, Institute of Physics, École Polytechnique Fédérale de Lausanne (EPFL), CH-1015 Lausanne, Switzerland*

[2]*Division of Materials Physics, Graduate School of Engineering Science, Osaka University, Toyonaka, Osaka 560-8531, Japan*

[3]*Department of Advanced Materials Science, University of Tokyo, Kashiwa 277-8561, Japan*

[4]*Laboratory for Neutron Scattering and Imaging, Paul Scherrer Institut, CH-5232 Villigen, Switzerland*

(Received 25 September 2017; revised manuscript received 22 November 2017; published 26 December 2017)

The antiferromagnetic compound $Ba(TiO)Cu_4(PO_4)_4$ contains square cupola of corner-sharing CuO_4 plaquettes, which were proposed to form effective quadrupolar order. To identify the magnetic structure, we have performed spherical neutron polarimetry measurements. Based on symmetry analysis and careful measurements, we conclude that the orientation of the Cu^{2+} spins form a noncollinear in-out structure with spins approximately perpendicular to the CuO_4 motif. Strong Dzyaloshinskii-Moriya interaction naturally lends itself to explain this phenomenon. The identification of the ground-state magnetic structure should serve well for future theoretical and experimental studies into this and closely related compounds.

DOI: 10.1103/PhysRevB.96.214436

The magnetoelectric effect, which describes the coupling between magnetism and ferroelectricity, allows for the ability to control the material's magnetization using an electric field or polarization using a magnetic field, making it a promising avenue for the next generation of data storage materials. A linear magnetoelectric effect in magnetically ordered systems necessitates the breaking of both the time reversal and the spatial inversion symmetry. The magnetic interaction energy of a magnetization density with an inhomogeneous magnetic field can be written as a multipole expansion containing monopole, toroid, and quadrupole moments, illustrated in Fig. 1 [1]. All three moments change sign under time reversal or space inversion as necessary for the linear magnetoelectric effect. Although toroidal multipole moments have been shown to possess magnetoelectric activity, the recently discovered $Ba(TiO)Cu_4(PO_4)_4$ is believed to be the first experimental observation of magnetoelectric activity originating from magnetic quadrupole moments [2,3].

The analysis of our previous powder neutron diffraction measurements was able to identify two possible models for the magnetic structure of $Ba(TiO)Cu_4(PO_4)_4$ [4]; however, it was limited by (i) weak magnetic Bragg reflections due to the small magnetic moment on Cu ions and (ii) the assumption of an isotropic magnetic form factor for Cu systems, which due to the nature of the electronic orbitals and covalency is typically not the case. To provide a solid footing for future experimental and theoretical studies, it is crucial to verify these results. The spherical neutron polarimetry (SNP) technique largely overcomes these problems, allowing for studies of magnetically ordered materials with magnetic moments of as small as $0.2\mu_B$ and providing polarization matrices that are unaffected by the magnetic form factors. To this end we have performed detailed SNP measurements, whose results are the focus of this article. Our findings are consistent with a strong Dzyaloshinskii-Moriya interaction as the driving mechanism for the unusual spin structure in $Ba(TiO)Cu_4(PO_4)_4$.

*peter.babkevich@gmail.com

I. SYMMETRY ANALYSIS

$Ba(TiO)Cu_4(PO_4)_4$ crystallizes in a chiral tetragonal structure with a space group $P42_12$ with lattice parameters of $a = 9.56$ Å and $c = 7.07$ Å [2]. The upward and downward square cupola of Cu_4O_{12} are arranged in an alternating fashion in the tetragonal ab plane [2], shown in Fig. 2. In between the Cu_4O_{12} cupola lies a nonmagnetic layer composed of tetrahedra of PO_4 and pyramids of TiO_5. The crystallographic unit cell contains eight Cu ions which are all equivalent to the general position (0.27,0.99,0.40). The magnetic structure of $Ba(TiO)Cu_4(PO_4)_4$ was previously studied in Ref. [4] using neutron powder diffraction. Antiferromagnetic order develops below $T_N = 9.5$ K, giving rise to magnetic reflections which can be indexed using a magnetic propagation wave vector $\mathbf{k} = (0,0,0.5)$. Group representation theory can be used to identify the possible magnetic structures emanating from the paramagnetic group from which the magnetic order emerges. A number of software packages are available to perform such an analysis, such as BASIREPS [5]. Below we outline the steps used to calculate the possible magnetic structures.

A. Representation analysis of magnetic structures

The little group $G_{\mathbf{k}}$ is a subset of symmetry elements within the paramagnetic space group G_0 ($P42_12$), which leaves the propagation wave vector invariant under the unitary transformation matrix M. In our case the little group contains all elements of G_0, which are listed in Table I. It is convenient to transform the representation of $G_{\mathbf{k}}$ into irreducible representations (IRs) which are orthogonal to one another.

The magnetic representation Γ_{mag} is the result of the symmetry operations on the position (polar) and spin (axial) vectors. The two are independent and can be treated separately. The former permutes the atomic positions $\mathbf{r}$ such that $g_n\mathbf{r}_i = \mathbf{r}_j$. The magnetic spin $\mathbf{S}$ must obey the axial vector property and remain invariant under an inversion, or $\mathbf{S}' = |M|M\mathbf{S}$. The magnetic representation is then a tensor product of the

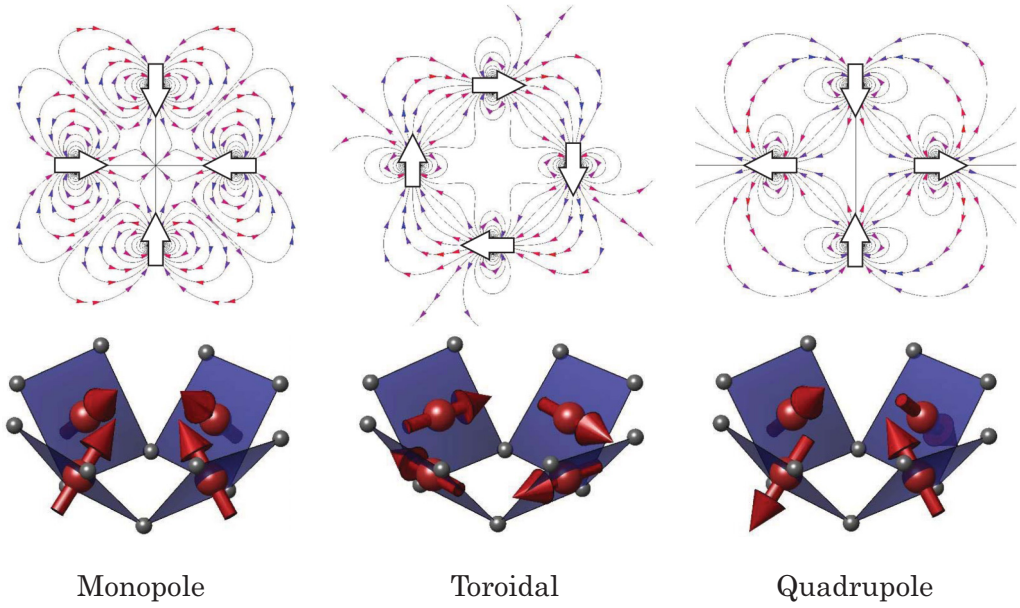

FIG. 1. Illustration of the arrangement of spins on the Cu_4O_{12} plaquette to produce an effective monopolar, toroidal, or quadrupolar moment in $Ba(TiO)Cu_4(PO_4)_4$.

permutation and axial representations,

$$\Gamma_{\text{mag}} = \Gamma_{\text{perm}} \times \Gamma_{\text{axial}}, \tag{1}$$

$$\chi_{\text{mag}} = \chi_{\text{perm}}\chi_{\text{axial}}. \tag{2}$$

The character χ of permutation and axial vector representations is simply given by the trace of the respective representations. Any magnetic representation is reducible to block-diagonal form by a summation over the IRs Γ_ν. The magnetic representation can then be described as

$$\Gamma_{\text{mag}} = \sum_\nu n_\nu \Gamma_\nu, \tag{3}$$

$$n_\nu = \frac{1}{n(G_{\mathbf{k}})} \sum_{g\in G_{\mathbf{k}}} \chi_{\text{mag}}(g)\chi_{\Gamma_\nu}(g)^*. \tag{4}$$

The value of n_ν tells us how many distinct basis vectors we can expect for each irreducible representation. In $Ba(TiO)Cu_4(PO_4)_4$, the magnetic representation at the Cu site with Wyckoff position $8g$ can be decomposed into a direct sum of irreducible representations as $\Gamma_{\text{mag}}(8g) = 3\Gamma_1 + 3\Gamma_2 + 3\Gamma_3 + 3\Gamma_4 + 6\Gamma_5^{(2)}$. All IRs are one-dimensional, except $\Gamma_5^{(2)}$, which is two-dimensional. The character table for $G_{\mathbf{k}}$ is given in Table II.

The basis vectors $\boldsymbol{\psi}$ are calculated using the projection operator technique by using a trial function along crystallographic axes $\boldsymbol{m}_a = (1,0,0)$, $\boldsymbol{m}_b = (0,1,0)$, and $\boldsymbol{m}_c = (0,0,1)$. The projection operator formula to find the basis vector $\boldsymbol{\psi}$ for magnetic representation Γ_ν is given as

$$\boldsymbol{\psi}_{\alpha\nu} = \sum_{g\in G_{\mathbf{k}}} \chi_\nu^*(g) \sum_n \delta_{n,g_n} |M(g)| M(g)\boldsymbol{m}_\alpha, \tag{5}$$

where $\chi(g)$ is the character of the little group $G_{\mathbf{k}}$. The spin distribution of the jth atom can be expressed as the Fourier transform of the linear combination of basis vectors, such that for a single propagation wave vector,

$$\mathbf{S}_j = \sum_n C_n \boldsymbol{\psi}_n e^{-i\mathbf{k}\cdot\mathbf{t}} + \text{c.c.}, \tag{6}$$

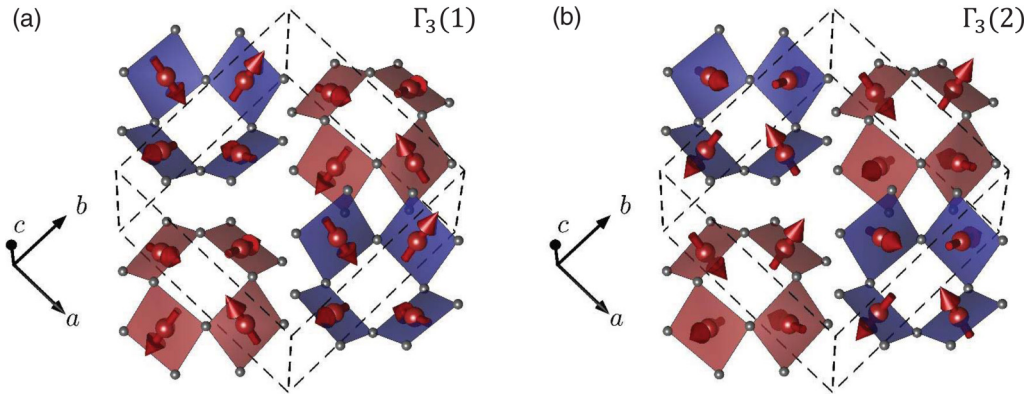

FIG. 2. Proposed magnetic structures described in the text of $Ba(TiO)Cu_4(PO_4)_4$ obtained from spherical neutron polarimetry. (a) Moments are lying almost in the CuO_4 planes. (b) Moments are almost perpendicular to CuO_4 planes.

TABLE I. Symmetry operators of space group $P42_12$ showing explicitly the rotational part M, IT notation as listed in the International Tables of Crystallography, and the Jones representation.

Element g_n	Rotation matrix M	IT notation	Jones symbol
g_1	$\begin{pmatrix}1&0&0\\0&1&0\\0&0&1\end{pmatrix}$	1	(x,y,z)
g_2	$\begin{pmatrix}\bar{1}&0&0\\0&\bar{1}&0\\0&0&1\end{pmatrix}$	2 0,0,z	$(-x,-y,z)$
g_3	$\begin{pmatrix}0&\bar{1}&0\\1&0&0\\0&0&1\end{pmatrix}$	4^+ 0,$\frac{1}{2}$,z	$(-y+1/2,x+1/2,z)$
g_4	$\begin{pmatrix}\bar{1}&0&0\\0&1&0\\0&0&\bar{1}\end{pmatrix}$	$2(0,\frac{1}{2},0)$ $\frac{1}{4}$,y,0	$(-x+1/2,y+1/2,-z)$
g_5	$\begin{pmatrix}0&1&0\\\bar{1}&0&0\\0&0&1\end{pmatrix}$	4^- $\frac{1}{2}$,0,z	$(y+1/2,-x+1/2,z)$
g_6	$\begin{pmatrix}1&0&0\\0&\bar{1}&0\\0&0&\bar{1}\end{pmatrix}$	$2(\frac{1}{2},0,0)$ x,$\frac{1}{4}$,0	$(x+1/2,-y+1/2,-z)$
g_7	$\begin{pmatrix}0&\bar{1}&0\\\bar{1}&0&0\\0&0&\bar{1}\end{pmatrix}$	2 x,$\bar{x}$,0	$(-y,-x,-z)$
g_8	$\begin{pmatrix}0&1&0\\1&0&0\\0&0&\bar{1}\end{pmatrix}$	2 x,x,0	$(y,x,-z)$

where the coefficients C_n can, in general, be complex. The magnetic moments obtained from the basis function calculated for the Γ_3 IR for the Cu sites resolved along crystallographic axes are

1. (u,v,w); 2. $(\bar{u},\bar{v},w)$; 3. $(v,\bar{u},\bar{w})$; 4. $(u,\bar{v},w)$;
5. $(\bar{v},u,\bar{w})$; 6. $(\bar{u},v,w)$; 7. $(\bar{v},\bar{u},\bar{w})$; 8. $(v,u,\bar{w})$.

The parameters u, v, and w are free parameters which are to be determined experimentally. Equivalent calculations can be made for the other IRs in $\Gamma_{\rm mag}$.[1] Rietveld refinement of the neutron powder diffraction data showed that Γ_3 gives the best agreement [4].

Within the Γ_3 IR, there exist two possible solutions which give a similar quality of fit to the observed magnetic diffraction powder pattern [4]. We label these models as Γ_3(1a) and Γ_3(2a) with magnetic moment components in units of μ_B, $(u,v,w) = [0.50(1),0.36(2),0.58(2)]$ and $[0.49(1),0.0(1),-0.62(2)]$, respectively. The magnetic structures of the two models closely resembles that illustrated in Fig. 2. We note that both Γ_3(1a) and Γ_3(2a) contain the component of the magnetic quadrupole moment which is illustrated in Fig. 1. In the case of Γ_3(1a) the moments are confined approximately in the plane of the CuO_4. Conversely, in the Γ_3(2a) model, the moments are approximately perpendicular to the CuO_4 planes and form a *two-in–two-out*–type arrangement within a Cu_4O_{12} plaquette. The goodness of fit to the powder neutron diffraction data was found to be slightly better for the Γ_3(2a) model. However, the refinement suffers from two problems. First, the magnetic form factor (see Sec. II) was assumed to be isotropic, which is typically not the case for Cu^{2+} ions. Furthermore, due to covalency, the magnetic form factor can be strongly modified [6]. Second, at larger $|\mathbf{Q}|$, the magnetic signal is rather weak due to the small magnetic moment of around 0.8 μ_B, and magnetic and structural Bragg peak overlap makes fitting difficult. Therefore, we turn to polarized neutron scattering to try to confirm and refine the complex, noncollinear magnetic structure found from powder neutron diffraction in Ba(TiO)$Cu_4(PO_4)_4$.

[1]The case of $\Gamma_5^{(2)}$ can produce a magnetic structure with an amplitude-modulated moment, which seems unlikely.

B. Domains

In order to accurately model the polarization matrices that are measured in spherical neutron polarimetry, we must consider the possible domains that could exist when the symmetry of the ordered magnetic structure is lower than that of the paramagnetic phase [7]. In the present case, we find that $G_{\mathbf{k}}$ contains all the symmetry elements of the paramagnetic space group. This means that translation symmetry is preserved on applying the symmetry operators and no configuration domains (or **k** domains) are produced.

An interesting property of Ba(TiO)$Cu_4(PO_4)_4$ is the chiral crystal structure in which there is no roto-inversion axis. In this case, a pair of enantimorphs can be formed that are related by a spatial inversion. A polarized light beam will be rotated when traversing through such a sample with the rotation being sensitive to the structural chirality. Indeed, such measurements have demonstrated the presence of structural chiral domains in Ba(TiO)$Cu_4(PO_4)_4$ [2].

II. MAGNETIC CROSS SECTION

In order to derive the polarization matrices, we present a brief account of the neutron scattering theory behind it [8–10]. The partial differential scattering cross section in an elastic neutron scattering measurement can be described by

$$\frac{\mathrm{d}\sigma}{\mathrm{d}\Omega} = \sum_{i,f} P(\lambda_i)|\langle\lambda_f,\sigma_f|\sum_j e^{i\mathbf{Q}\cdot\mathbf{r}_j}U_j|\lambda_i,\sigma_i\rangle|^2\delta(E). \quad (7)$$

This gives the probability that a neutron is scattered into a solid angle Ω without transferring any energy to the system. The initial (final) states of the neutron and sample are given by σ_i and λ_i (σ_f and λ_f), respectively. The statistical weight factor for an initial state $|\lambda_i\rangle$ is given by $P(\lambda_i)$. The last term ensures energy conservation during the scattering process, which in the present case will be restricted to purely elastic scattering. The atomic scattering amplitude for the jth atom at position $\mathbf{r}_j$ is given as

$$U_j = b_j^{\rm coh} + \frac{b_j^{\rm inc}}{\sqrt{I(I+1)}}\mathbf{I}_j\cdot\boldsymbol{\sigma} - p_j\mathbf{S}_{\perp j}\cdot\boldsymbol{\sigma}. \quad (8)$$

The scattering length operator for the interaction between neutrons and nuclei consists of both coherent and incoherent scattering lengths b which can contribute to the total scattering cross section. The Pauli spin operator $\boldsymbol{\sigma}$ is the normalized neutron spin operator and the nucleus spin operator is **I**.

TABLE II. Matrix representation of the IRs with respect to the symmetry operations $g_1,\ldots,g_8$ in Table I. The final column gives the magnetic space group of each IR in the Belov-Neronova-Smirnova notation.

ν	g_1	g_2	g_3	g_4	g_5	g_6	g_7	g_8	MSG
1	1	1	1	1	1	1	1	1	$P42_12$
2	1	1	1	1	$\bar{1}$	$\bar{1}$	$\bar{1}$	$\bar{1}$	$P42_121'$
3	1	1	$\bar{1}$	$\bar{1}$	1	1	$\bar{1}$	$\bar{1}$	$P42_121'$
4	1	1	$\bar{1}$	$\bar{1}$	$\bar{1}$	$\bar{1}$	1	1	$P4'2'_12$
5	$\begin{pmatrix}1&0\\0&1\end{pmatrix}$	$\begin{pmatrix}\bar{1}&0\\0&\bar{1}\end{pmatrix}$	$\begin{pmatrix}1&0\\0&\bar{1}\end{pmatrix}$	$\begin{pmatrix}\bar{1}&0\\0&1\end{pmatrix}$	$\begin{pmatrix}0&1\\1&0\end{pmatrix}$	$\begin{pmatrix}0&\bar{1}\\\bar{1}&0\end{pmatrix}$	$\begin{pmatrix}0&\bar{1}\\1&0\end{pmatrix}$	$\begin{pmatrix}0&1\\\bar{1}&0\end{pmatrix}$	–

The last term in Eq. (8) describes the magnetic scattering of the neutrons by the sample. The factor $p=(\gamma r_0)f(\mathbf{Q})/2$ for a spin-only moment, where the gyromagnetic ratio $\gamma=1.913$ and the classical electron radius $r_0=2.82$ fm. The magnetic form factor $f(\mathbf{Q})$ corresponds to the Fourier transform of the unpaired spin density on an atom. The magnetic interaction vector, $\mathbf{S}_\perp=\hat{\mathbf{Q}}\times\mathbf{S}\times\hat{\mathbf{Q}}$, expresses the fact that only magnetization perpendicular to $\mathbf{Q}$ can scatter neutrons. In the case of coherent magnetic scattering of unpolarized neutrons from a magnetically ordered crystal, the elastic differential scattering cross section is derived from Eqs. (7) and (8) as

$$\frac{\mathrm{d}\sigma}{\mathrm{d}\Omega}\propto|\mathbf{F}(\mathbf{Q})|^2\delta(\mathbf{Q}+\mathbf{G}\pm\mathbf{k}) \tag{9}$$

for a given propagation wave vector $\mathbf{k}$ and reciprocal lattice wave vector $\mathbf{G}$. The structure factor is found as

$$\mathbf{F}(\mathbf{Q})=\sum_j p_j\langle\mathbf{S}_{\perp j}\rangle e^{i\mathbf{Q}\cdot\mathbf{r}_j}e^{-W_j}, \tag{10}$$

which includes the Debye-Waller factor e^{-W_j}, and $\langle\mathbf{S}_\perp\rangle$ contains the thermally averaged expectation value of the spin perpendicular to $\mathbf{Q}$.

A. Polarized neutron scattering

Polarized neutron scattering makes use of the incident and outgoing neutron spin state to provide additional information about the magnetic system. The polarization of a neutron beam is a statistical quantity defined as the expectation value of an ensemble of neutron spins. The scattering of a neutron from a sample can in general reorient the neutron moment from one orientation to any other in three dimensions. This process can be neatly described by a polarization matrix $P_{\alpha\beta}$, which consists of measuring 18 different scattering intensities in the spin-flip and non-spin-flip channels, $\sigma(\alpha,\beta)$ and $\sigma(\alpha,-\beta)$, respectively. The initial spin direction is defined by α and the final direction by β, such that,

$$P(\alpha,\beta)=\frac{\sigma(\alpha,\beta)-\sigma(\alpha,-\beta)}{\sigma(\alpha,\beta)+\sigma(\alpha,-\beta)}. \tag{11}$$

In neutron polarimetry, it is useful to define x as parallel to $\mathbf{Q}$, z perpendicular to the scattering plane, and y completes the right-handed coordinate system. The α and β are defined in this coordinate system,

$$|x\rangle=\frac{1}{\sqrt{2}}\begin{pmatrix}1\\1\end{pmatrix},\quad |y\rangle=\frac{1}{\sqrt{2}}\begin{pmatrix}1\\i\end{pmatrix},\quad |z\rangle=\begin{pmatrix}1\\0\end{pmatrix},$$
$$|\bar{x}\rangle=\frac{1}{\sqrt{2}}\begin{pmatrix}1\\\bar{1}\end{pmatrix},\quad |\bar{y}\rangle=\frac{1}{\sqrt{2}}\begin{pmatrix}1\\\bar{i}\end{pmatrix},\quad |\bar{z}\rangle=\begin{pmatrix}0\\1\end{pmatrix}.$$

From Eqs. (7) and (8) we will in general obtain nuclear, magnetic or a mix of nuclear-magnetic interference terms upon squaring. However, for present case of $Ba(TiO)Cu_4(PO_4)_4$, the magnetic propagation wave vector is (0,0,0.5) and therefore the magnetic and nuclear reflections will occur at different positions in reciprocal space.

The neutron and electron (which is responsible for the magnetization) coordinates are independent, which allows us to separate the matrix element in Eq. (7) to $\langle\sigma_\mathrm{f}|\boldsymbol{\sigma}|\sigma_\mathrm{i}\rangle\langle\lambda_\mathrm{f}|\sum_j e^{i\mathbf{Q}\cdot\mathbf{r}_j}p_j\mathbf{S}_\perp|\lambda_\mathrm{i}\rangle$, where the second term is equivalent to $\mathbf{F}(\mathbf{Q})$ in Eq. (10). We define $\mathbf{F}(\mathbf{Q})=(0,F_y,F_z)$, resolved along our chosen coordinate system $\{x,y,z\}$. Due to the cross product in $\mathbf{S}_\perp$, the contribution of magnetization along x is zero. Therefore, we can define the scattering cross sections in Eq. (11) as

$$\sigma(\alpha,\beta)\propto|\langle\beta|\begin{pmatrix}F_z&-iF_y\\iF_y&-F_z\end{pmatrix}|\alpha\rangle|^2. \tag{12}$$

Since the matrix is measured at a particular $\mathbf{Q}$ point and consists of normalized intensity in Eq. (11), the polarization analysis is not sensitive to the magnetic form factor contained in p_j, nor to the size of the magnetic moment. In practice, measuring magnetic Bragg peaks at larger $|\mathbf{Q}|$ becomes increasingly challenging as the magnetic form factor decreases the scattering intensity. For the special case of longitudinal neutron polarimetry at $\mathbf{Q}=\mathbf{G}+\mathbf{k}$,

$$\sigma(x,x)=0,\qquad \sigma(x,\bar{x})=|\mathbf{F}|^2+i(\mathbf{F}\times\mathbf{F}^*),$$
$$\sigma(y,y)=|F_y|^2,\qquad \sigma(y,\bar{y})=|F_z|^2,$$
$$\sigma(z,z)=|F_z|^2,\qquad \sigma(z,\bar{z})=|F_y|^2.$$

TABLE III. The Cu spin direction has been obtained by fitting the spherical neutron polarimetry data. The moment direction (u,v,w) are normalized to the moment size m_0 obtained from fitting WISH powder data. The refined levo chiral domain population is also shown. The values in parentheses indicate 1-standard-deviation uncertainties in the fit parameters.

SNP	Γ_3(1b)	Γ_3(2b)
u (μ_B)	0.56(2)	0.56(2)
v (μ_B)	−0.01(1)	0.03(1)
w (μ_B)	0.59(2)	−0.57(2)
m_0 (μ_B)	0.81(1)	0.80(1)
Levo domain	64(7)%	36(7)%
χ^2_ν	18.9	18.9

We note that the $\sigma(x,\bar{x})$ is sensitive to a chiral magnetic structure through the term $i(\mathbf{F}\times\mathbf{F}^*)$. In the case of perfect beam polarization and a single-domain structure, the polarization matrix can be found as

$$P = \begin{pmatrix} -1 & 0 & 0 \\ C & -A & B \\ C & B & A \end{pmatrix}, \tag{13}$$

$$\begin{aligned} AD &= |F_z|^2 - |F_y|^2, \\ BD &= F_y F_z^* + F_y^* F_z, \\ CD &= i(F_y F_z^* - F_y^* F_z), \\ D &= |F_y|^2 + |F_z|^2. \end{aligned} \tag{14}$$

The $P(x,x)$ element readily identifies the nature of the reflection: $P(x,x) = +1$ for a nuclear Bragg peak and $P(x,x) = -1$ for a magnetic one. The coherent scattering from the nuclear structure does not contain any spin dependence in Eq. (8), which means that the initial spin state of the neutron will be preserved after scattering from the nuclear structure. This is an important consequence for polarized neutron scattering, which allows us to cleanly separate the signal originating from coherent nuclear or magnetic scattering processes. It should be noted that the nuclear spin incoherent scattering can flip the spin and thereby contribute to a featureless spin-flip background.

The chiral term in Eq. (14) can be equivalently expressed as $CD = i(\mathbf{F}\times\mathbf{F}^*)$ and is a signature of noncollinear magnetic order. For a single domain, the summation $A^2 + B^2 + C^2 = 1$ will hold for ideal beam polarization. Magnetic domains can depolarize the neutron beam such that $A^2 + B^2 + C^2 \leqslant 1$. Symmetry consideration are necessary to account for this.

In the 1960s, Blume and Maleyev established equations that were useful in gaining insight into how the different scattering processes affect the different elements of the polarization matrix [11,12]. However, this formulation was restricted to the single-domain case only, which does not hold true for most magnetic systems. Herein we shall outline the methodology for treating multidomain structures. In the case of a multidomain sample, the scattering cross section in Eq. (11) becomes

$$\sigma(\alpha,\beta) \to \sum_n f_n \sigma_n(\alpha,\beta), \tag{15}$$

where the fraction of the nth domain is given by f_n.

B. Imperfect beam polarization correction

In practice, 100% neutron spin polarization is not possible. The incident and scattered beam will have a polarization efficiency of $0 < \eta_i, \eta_f < 1$. This will cause some neutrons to scatter into the wrong channel, which needs to be corrected when comparing measured matrices with the calculated ones. For a measured scattering cross section $\sigma_m(\alpha,\beta)$, we must consider an ensemble average of $\eta_i|\alpha\rangle$ neutrons with the correct polarization and $(1-\eta_i)|-\alpha\rangle$ with the wrong polarization. Considering similarly the out-going neutron beam polarization gives the corrected scattering cross section as

$$\begin{aligned} \sigma_c(\alpha,\beta) = {} & \eta_i\eta_f\sigma(\alpha,\beta) + \eta_i(1-\eta_f)\sigma(\alpha,-\beta) \\ & + (1-\eta_i)\eta_f\sigma(-\alpha,\beta) \\ & + (1-\eta_i)(1-\eta_f)\sigma(-\alpha,-\beta). \end{aligned} \tag{16}$$

Similarly, by setting $\alpha \to -\alpha$ and/or $\beta \to -\beta$ one can obtain the scattering cross section for other channels. A good estimate of the polarization efficiencies can be obtained by measuring a Bragg reflection which is either purely nuclear or magnetic in origin. It is useful to define the spin-flip ratio R, which for a nuclear reflection and $\eta_i = \eta_f = \eta$ is

$$R = \left(\frac{\sigma_{NSF}}{\sigma_{SF}}\right)_m = \frac{1}{2\eta(1-\eta)} - 1, \tag{17}$$

by measuring the ratio of the intensities in the spin-flip (SF) and non-spin-flip (NSF) channels. A flipping ratio of 12 will correspond to a neutron beam polarization efficiency of 96%. However, some caution needs to be taken, particularly when working on systems with short-range magnetic order with a focusing monochromator and/or analyzers, as R for nuclear resolution-limited reflections can be somewhat higher than diffuse magnetic scattering owing to spatial distribution of the neutron beam polarization.

III. EXPERIMENTAL RESULTS

A. Experimental setup

Spherical neutron polarimetry measurements were performed using the MuPAD configuration of the TASP spectrometer configuration at SINQ [13–15]. Incident neutrons of wavelength 1.97 $Å^{-1}$ were used for the measurements. A single-crystal Ba(TiO)$Cu_4(PO_4)_4$ sample of 0.6 g grown by the flux method [2] was mounted on an Al holder. Measurements of the flipping ratio were performed on the (200), (220), and (002) nuclear reflections, giving $R = 13.2$ corresponding to $\eta_i = \eta_f = 96.4\%$. The modeled polarization matrices take this nonideal beam polarization into account as defined in Eq. (16). Two sample orientation geometries were used to access the $(h0l)$ and (hhl) scattering planes. Complete normal $P(\alpha,\beta)$ and negative $P(-\alpha,\beta)$ polarization matrices were recorded at 1.5 and 20 K to eliminate the contributions from the systematic errors and background. In total, 26 polarization matrices were used in the analysis, with around 1 hour counting time per matrix.

B. Polarization matrix simulations

Figure 3 illustrates some of the polarization matrices recorded. We note that in our data $P(y,x) \neq P(z,x)$ and for some reflections $P(x,z) \neq 0$. These are probably caused by small gaps in the mu-metal shielding, which results in systematic errors. To mitigate these errors, we have collected equivalent reflections and measured negative polarization matrices. An alternate scenario could be that there is a small amount of nuclear-magnetic interference, perhaps originating from some sort of a superstructure; however, our data is insufficient to provide further insight.

No magnetic intensity was found for reflections $(0,0,0.5) + (0,0,l)$ for $l = 0,1,2$. One might naively expect this to reflect that spins are all parallel to the c axis. However, this can

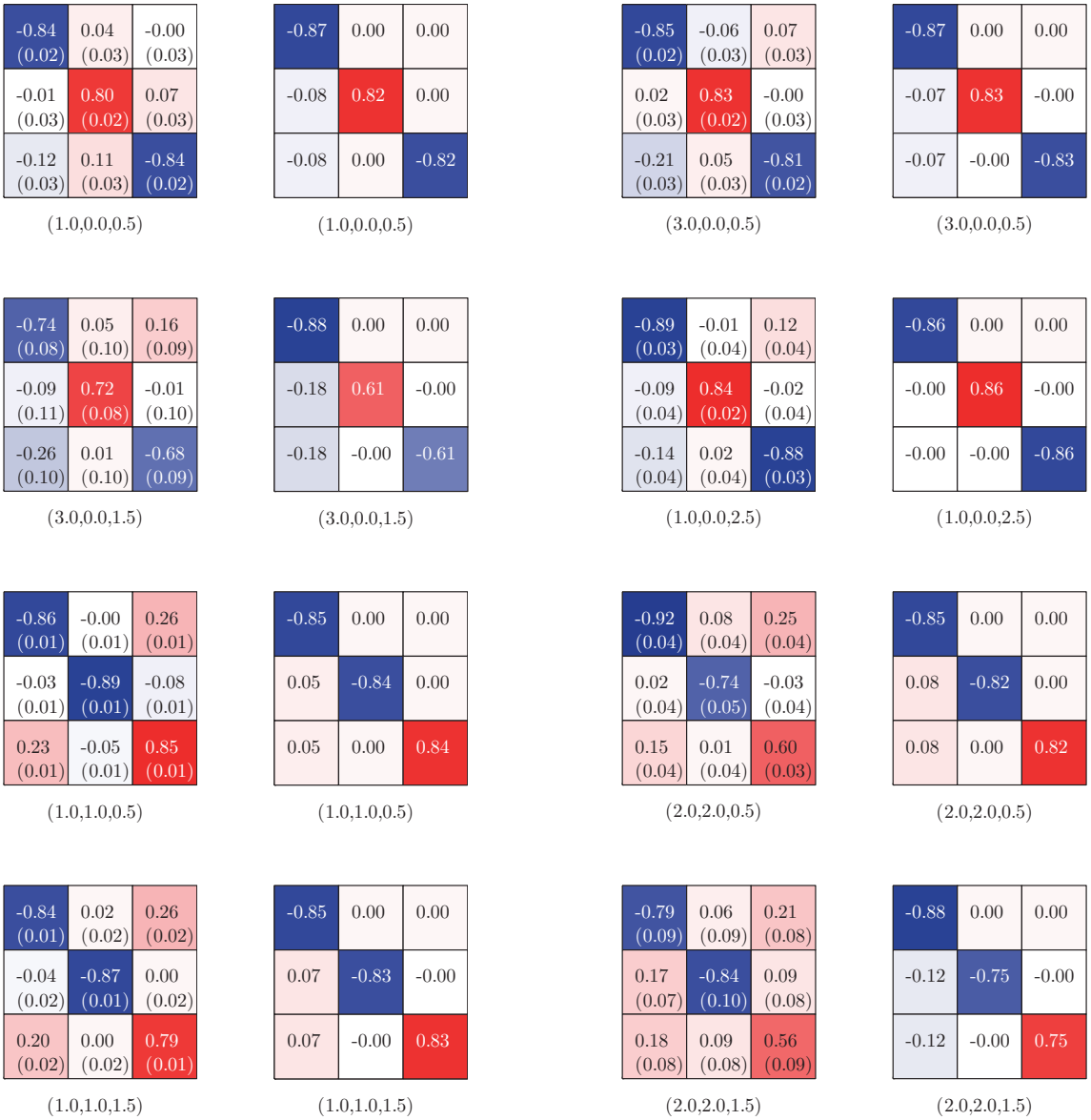

FIG. 3. A selection of the polarization matrices recorded for different (hkl) positions indicated below the polarization matrices. Blue, white, and red colors represent $P(\alpha,\beta) = -1, 0$, and $+1$, respectively. Uncertainty in the matrix element is given in parenthesis. A background collected at 20 K has been removed from the data measured at 1.5 K. Matrices without parenthesis indicate simulation matrices. The simulated polarization matrices were calculated for the Γ_3(2b) magnetic structure given in Table III. A correction for beam polarization efficiency of 96.4% has been applied to the calculated polarization matrices.

be easily shown not to hold true. If we examine the $P(y,y)$ and $P(z,z)$ elements at (1,1,0.5), for example, we find measured values of $-0.89(1)$ and $+0.85(1)$, respectively (see Fig. 3). Assuming a beam polarization efficiency of 96.4% and spins along the c axis results in $P(y,y) = +0.86$ and $P(z,z) = -0.86$, i.e., exactly opposite to what we observe experimentally. Indeed, a very poor goodness of fit to the complete data set of $\chi^2_\nu = 2000$ is found for such a model.

A key advantage of symmetry analysis is that it greatly reduces the number of free parameters. In the case of $Ba(TiO)Cu_4(PO_4)_4$ we are left, for each possible IR, with a refinement of three parameters: the polar and zenith angles of the Cu spin and the levo-dextro domain population. We treat levo as the domain in which Cu ion is situated at (0.27,0.99,0.40) and dextro as the structural chiral domain related by a spatial inversion. Fitting the complete set of the polarization matrices that have been collected, we find two possible solutions, shown in Table IV, with identical quality of fit of $\chi^2_\nu = 18.9$.[2] The measured and simulated polarization matrices for the Γ_3(2b) structure are shown in Fig. 3. The two magnetic structure solutions are shown in Fig. 2. We note that our SNP measurements differ from those obtained previously from neutron powder diffraction [4]. In the case of Γ_3(1b),

[2]We note that the χ^2_ν only includes the random errors and not the systematic ones, resulting in values somewhat larger than 1.

TABLE IV. Results of magnetic structure refinement based on neutron powder diffraction (ND) measurements obtained from the WISH and D20 diffractometers and single-crystal spherical neutron polarimetry (SNP) for the two proposed magnetic structures. In the case of SNP+ND, the magnetic structure from SNP was used but the moment size was refined using ND data. The SNP+ND(WISH) corresponds to the goodness of fit for the diffraction patterns obtained from the two detector banks covering the smallest $|\mathbf{Q}|$ range.

	Γ_3(1b)	Γ_3(2b)
ND(D20)	16.4%	11.4%
SNP+ND(D20)	32.6%	18.8%
ND(WISH)	18.5%	11.5%
SNP+ND(WISH)	(35.5%, 42.9%)	(18.0%, 14.3%)

SNP finds the moment along the b axis is nearly zero compared to 0.36(2) μ_B. The magnetic structure from SNP, Γ_3(2b), is nearly the same as Γ_3(1b), with the exception that SNP is able to reduce the uncertainty in the b component. Γ_3(1b) is characterized by spins lying in the CuO_4 plane (within about 5°), while in Γ_3(2b) they are nearly perpendicular to the plane, being approximately 5° from the normal of the CuO_4 plane. It is interesting to note that Γ_3(1b) can be mapped into Γ_3(2b) spin structures, and vice versa, by displacing the atomic structure by (0.5,0.5,0.2). If the c-axis component were zero, the magnetic structure factors of the two models would be the same; however, this small shift along the c axis between the Cu_4O_{12} plaquettes gives a discernible, albeit small difference between the two models.

To elucidate the magnetic structure of $Ba(TiO)Cu_4(PO_4)_4$, we return to neutron powder diffraction measurements. Two experiments have been carried out so far on the same $Ba(TiO)Cu_4(PO_4)_4$ powder sample using D20 at ILL and WISH at ISIS diffractometers, whose results are reported elsewhere [4,16]. In Table IV we present the goodness-of-fit values obtained by either fitting the data, allowing the moment size and direction to vary, or fixing the moment direction as obtained from spherical neutron polarimetry. We find that in each case there is a better fit obtained for the Γ_3(2b) spin structure. The calculations were performed assuming an isotropic magnetic form factor. We stress that it is not known in which orbital the electron is in, nor the extent of covalent bonding that is often found for Cu-based compounds. Both of these effects have potentially significant effects on the magnetic form factor and hence the magnetic structure factor. As previously described, spherical neutron polarimetry eliminates this problem, and as a result we have more confidence in the spin structure obtained in $Ba(TiO)Cu_4(PO_4)_4$.

Let us consider just the nearest-neighbor Cu spins, as depicted in Fig. 4. We note that the dominant exchange path between Cu ions is likely to be through the shared O atom. The large displacement of the O from the line connecting Cu-Cu sites [see Fig. 4(c)] implies first that the superexchange interaction J is likely to be small, and second that the Dzyaloshinskii-Moriya (DM) interaction could be strong [17,18]. The antiferromagnetic exchange interaction encourages the spins to be antiparallel, while the DM interaction would favor a noncollinear spin arrangement. For two spins, the DM interaction has the

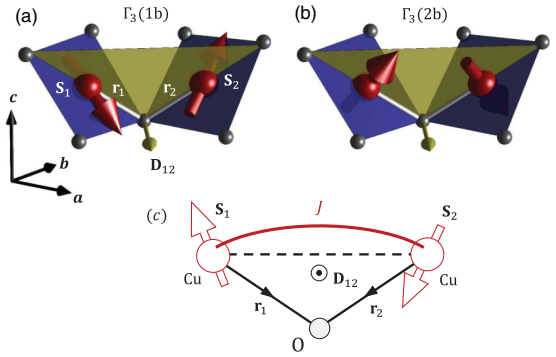

FIG. 4. Illustration of the DM interaction at play in $Ba(TiO)Cu_4(PO_4)_4$. Panels (a) and (b) show the nearest-neighbor Cu spins, each connected to 4 O atoms in the case of Γ_3(1b) and Γ_3(2b) spin structures. The yellow plane represents the normal to the Cu-O-Cu bond, with the direction of the DM vector shown in yellow. (c) Simplified diagram to illustrate the DM interaction.

form

$$\mathcal{H}_{\mathrm{DM}} = -\mathbf{D}_{12} \cdot (\mathbf{S}_1 \times \mathbf{S}_2), \tag{18}$$

where the DM vector $\mathbf{D}_{12} \propto \lambda \mathbf{r}_1 \times \mathbf{r}_2$ and λ is the spin-orbit coupling. The vector connecting Cu and O is given by $\mathbf{r}$. In the case of $Ba(TiO)Cu_4(PO_4)_4$, we would expect the DM vector to be mostly in the ab plane, as shown in Figs. 4(a) and 4(b). The most energetically favorable spin configuration in the presence of strong DM interaction would be where the spins lie in the plane normal to $\mathbf{D}_{12}$. This scenario is realized for the case of the Γ_3(2b) model where the spins are found to be almost normal to $\mathbf{D}_{12}$, see Fig. 4(b). For Γ_3(1b), the $\mathbf{S}_1 \times \mathbf{S}_2$ vector is approximately 130° from $\mathbf{D}_{12}$, while for Γ_3(2b) this is just 20°. Therefore, we would naively expect the DM interaction to stabilize the Γ_3(2b) rather than the Γ_3(1b) spin structure. A large DM interaction contribution has been proposed theoretically for $Ba(TiO)Cu_4(PO_4)_4$ to reproduce the bulk magnetization measurements [3]. Moreover, inelastic neutron scattering measurements on $Ba(TiO)Cu_4(PO_4)_4$ show a large spin gap relative to the total bandwidth of the magnetic excitations [4]; these results would be consistent with the present scenario where a strong DM interaction is responsible for the anisotropy and large spin gap and demonstrates that our results are consistent.

IV. CONCLUSIONS

Spherical neutron polarimetry is a powerful technique for probing systems where structural and magnetic signals are intertwined and/or magnetic structure is noncollinear. While standard methods of single-crystal and powder diffraction are able to shed light on magnetic ordering of systems, neutron polarimetry can in certain cases be significantly more efficient and robust. We have employed spherical neutron polarimetry to show that in $Ba(TiO)Cu_4(PO_4)_4$ there are two possible magnetic spin structures. In combination with previously recorded neutron powder diffraction, we find that in $Ba(TiO)Cu_4(PO_4)_4$, the Cu spins are arranged in two-in–two-out manner with spins pointing approximately perpendicular

to the CuO_4 motif. This spin structure is consistent with a strong DM interaction, which naturally explains the large spin gap observed in the magnetic spectrum of $Ba(TiO)Cu_4(PO_4)_4$ [4]. Given the rich physics in the $A(BO)Cu_4(PO_4)_4$ family [16], our measurements should pave the way for future experimental and theoretical investigations of these intriguing materials.

ACKNOWLEDGMENTS

The study was supported by the Swiss National Science Foundation (SNSF) and its Synergia network Mott Physics Beyond the Heisenberg Model (MPBH). K.K. is grateful for the funding received from the Japan Society for the Promotion of Science through Grant No. 16K05449 and a research grant from The Murata Science Foundation.

[1] N. A. Spaldin, M. Fiebig, and M. Mostovoy, J. Phys.: Condens. Matter **20**, 434203 (2008).
[2] K. Kimura, M. Sera, and T. Kimura, Inorg. Chem. **55**, 1002 (2016).
[3] Y. Kato, K. Kimura, A. Miyake, M. Tokunaga, A. Matsuo, K. Kindo, M. Akaki, M. Hagiwara, M. Sera, T. Kimura, and Y. Motome, Phys. Rev. Lett. **118**, 107601 (2017).
[4] K. Kimura, P. Babkevich, M. Sera, M. Toyoda, K. Yamauchi, G. S. Tucker, J. Martius, T. Fennell, P. Manuel, D. D. Khalyavin, R. D. Johnson, T. Nakano, Y. Nozue, H. M. Rønnow, and T. Kimura, Nat. Commun. **7**, 13039 (2016).
[5] J. Rodriguez-Carvajal, Physica B **192**, 55 (1993).
[6] A. C. Walters, T. G. Perring, J.-S. Caux, A. T. Savici, G. D. Gu, C.-C. Lee, W. Ku, and I. A. Zaliznyak, Nat. Phys. **5**, 867 (2009).
[7] T. Chatterji, *Neutron Scattering from Magnetic Materials* (Elsevier, Amsterdam, 2006).
[8] G. L. Squires, *Introduction to the Theory of Thermal Neutron Scattering* (Cambridge University Press, Cambridge, UK, 2012).
[9] G. Shirane, S. M. Shapiro, and J. M. Tranquada, *Neutron Scattering With a Triple-Axis Spectrometer: Basic Techniques* (Cambridge University Press, New York, 2002).
[10] B. Roessli and P. Böni, *Polarized Neutron Scattering. Scattering and Inverse Scattering in Pure and Applied Science* (Academic Press, New York, 2002).
[11] M. Blume, Phys. Rev. **130**, 1670 (1963).
[12] Y. Izyumov and S. Maleyev, Sov. Phys. JETP **14**, 1168 (1962).
[13] W. E. Fischer, Physica B **234**, 1202 (1997).
[14] F. Semadeni, B. Roessli, and P. Böni, Physica B **297**, 152 (2001).
[15] M. Janoschek, S. Klimko, R. Gähler, B. Roessli, and P. Böni, Physica B **397**, 125 (2007).
[16] K. Kimura, M. Toyoda, P. Babkevich, K. Yamauchi, M. Sera, V. Nassif, H. M. Rønnow, and T. Kimura (unpublished).
[17] I. Dzyaloshinsky, J. Phys. Chem. Solids **4**, 241 (1958).
[18] T. Moriya, Phys. Rev. **120**, 91 (1960).